Int J Adv Manuf Technol
DOI 10.1007/s00170-015-8293-6

ORIGINAL ARTICLE

Estimation of temperature-dependent heat transfer coefficients in near-dry cutting

Feng Jiang[1] · **Tao Zhang**[1] · **Lan Yan**[2]

Received: 12 October 2015 / Accepted: 21 December 2015
© Springer-Verlag London 2016

Abstract Cutting fluid is the most common method to control the cutting temperature. However, it is usually harmful to the environment and personal health. Near-dry cutting could be an effective substitute of cutting fluid. Most researchers focus on the lubrication during near-dry cutting processes. Actually, the cooling ability of near-dry cutting is very important for the control of cutting temperature and effectiveness of coolant. In this study, heat transfer coefficients (HTCs) of different cooling processes, including nature cooling, compressed air cooling, compressed cold air cooling, minimal quantity lubrication (MQL) cooling, and atomizing water cooling, have been estimated. Surface temperature, temperature of coolant carrier, and air velocity of coolant carrier have a great effect on the cooling ability of near-dry cutting system. The finite element method (FEM) is employed to simulate the cooling process and modify the estimated heat transfer coefficients. It is found that HTC is from 9.3 to 53.9 W/m^2/°C with different surface temperatures in nature cooling. HTC increases with the increase of surface temperature. HTC is from 48.1 to 346.0 W/m^2/°C with different air velocity and surface temperature in compressed air cooling. HTC has an increased trend with the increase of air velocity. HTC is from 52.6 to 405.6 W/m^2/°C with different air velocities and surface temperatures in compressed cold air cooling. Lower air temperature increases HTC by 10~20 %. HTC is from 96.5 to 718.7 W/m^2/°C with different oil quantities and surface temperatures in MQL cooling. HTC increases with the increase of oil quantity of MQL. As a comparison, HTC is from 133.7 to 519.6 W/m^2/°C with different water quantities and surface temperatures in atomizing water lubrication (AWL) cooling. HTC of AWL is much lower than that of MQL in the same condition, especially when the surface temperature is high. The boiling point of water is much lower than oil; subsequently, less water mist arrives at the cooled surface, so less heat is removed with AWL cooling than that with MQL cooling in the same condition. HTC is from 282.1 to 1890.3 W/m^2/°C with different oil quantities and surface temperatures in cold-air MQL cooling. Lower carrier temperature increases the HTC greatly, even increases the HTC by 150 % when the surface temperature is up to 700 °C. The reason is that the coolant prevents high-temperature deterioration before the coolant arrives at a cooled surface.

Keywords Temperature-dependent heat transfer coefficient · Near-dry cutting · Infrared pyrometer · Finite element analysis

✉ Feng Jiang
jiang.feng.sdu@gmail.com

Tao Zhang
zhangtao.ime@hqu.edu.cn

Lan Yan
yanlan@hqu.edu.cn

[1] Institute of Manufacturing Engineering, Huaqiao University, 361021 Xiamen, People's Republic of China

[2] College of Mechanical Engineering and Automation, Huaqiao University, 361021 Xiamen, People's Republic of China

1 Introduction

Using cutting fluid is the most common strategy to control the cutting temperature, but it also brings in environmental and cost concerns. In addition, it has been pointed out that cutting fluid, especially water-soluble coolant, may lead to hydrogenation and oxidation of some workpiece and cutting tool materials, which result in chipping at the cutting edge and fracture on the rake face of the cutting tool [1]. Near-dry cutting

Published online: 05 January 2016

Table 1 The HTC values obtained under different conditions

Manufacturing processes	Cooling method	Estimation method	HTC (W/m^2 K)	Cooling media	Literature
Grinding	Flooding	Analytical	43,400	5 % synthetic	[12]
	MQL	Analytical	1400 to 1630	100 % mineral	[12]
			1450	100 % hydrocracked	[12]
Tapping/drilling	Flooding	Inverse	10,000	100 % mineral	[15]
		Analytical	3218	100 % mineral	[16]
	MQL	Inverse	100	100 % mineral	[15]
		Analytical	3555	100 % mineral	[16]
	Dry	Inverse	100	Natural air	[15]
		Analytical	3207	Natural air	[16]
Turning	Flooding	Analytical	3811	59 % mineral	[17]
			5310	45 % vegetable	
		Inverse	2500	Water-based coolant	[18]
	MQL	Analytical	678	100 % mineral	[17]
			454	83 % vegetable	
	Compressed air	Analytical	36.8 to 355 in the different air pressure and surface temperature	Compressed cold air with temperature −20 °C	[19]
	Dry	Analytical	122	Natural air	[17]
			9.32 to 55.1 in the different surface temperature	Natural air	[19]
		Finite element	4 to 320 with different cutting speed and feed rate	Natural air	[20]
		Inverse	22.6	Natural air	[18]
Milling	Dry	Finite element	436-1372 with different thermal models and cutting speed	Natural air	[21]
		Finite element	500 to 1000 with different milling tool and workpiece materials	Natural air	[22]
	Compressed air	Finite element	2500 with different milling tool and workpiece materials	Compressed air of 0.6 MPa	[22]
		Finite element	10,000 to 50,000 with different milling tool and workpiece materials	Compressed cold air of 0.6 MPa and −2 °C	[22]
Wire electro-discharge	Wet	Analytical	13,420 to 18,234 with different peak current and flushing pressure	WEDM coolant	[23]

method, including minimal quantity lubrication (MQL) machining [2], atomizing water lubrication (AWL) machining [3], cold-air machining [4], cryogenic machining [5], and so on, is an effective substitute of conventional cutting fluid. Near-dry cutting technique could enhance cutting performance in terms of increasing tool life and improving the quality of the machined surface [6]. It is found that the cutting temperature in near-dry cutting is even lower than that in wet cutting when fluid nozzle position and cutting parameters are optimized [7]. Furthermore, cold air is used as the carrier of cutting fluid to decrease the effect of cutting temperature on cutting fluid [4]. It is found that the cooling intensity of compressed air cooling with air temperature −40 °C is about 10 % more than the cooling intensity of compressed air cooling with air temperature 20 °C [8]. And the oil mist with cold air as a carrier prevents effectiveness lose due to high cutting temperature [9].

Most researchers consider that the performance improvement of near-dry cutting is due to better lubrication, especially enhanced penetration of lubricant into the cutting zone [10]. Actually, the cooling ability of the carrier is very important to keep the performance of cutting fluid as well as lower the cutting temperature [11]. It is found that the cooling intensity of compressed air cooling with air velocity 500 m/s is about 50 % of the cooling intensity of water cooling with water speed 0.2 m/s [8]. And the cooling ability of near-dry cutting system is limited by the thermal properties, diameter of mist nozzle, flow rate, and air pressure of homogeneous fluid [12]. Heat transfer coefficient (HTC) could be a reasonable index to measure cooling ability. And HTC is an important input

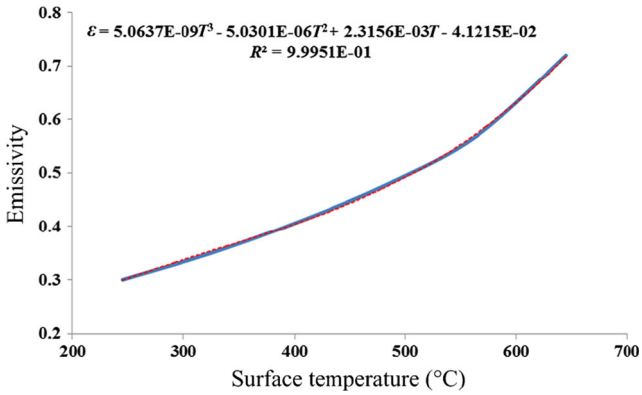

Fig. 1 Temperature-dependent emissivity of cemented carbide

parameter in numerical simulation of heat transfer process, including the prediction of cutting temperature [13, 14]. Heat transfer coefficient in the machining process could be obtained by analytical model, inverse method, and finite element method (FEM). The HTC value of different machining processes is listed in Table 1.

However, the heat transfer coefficients obtained from different estimation methods and different machining processes exist in great differences, as shown in Table 1. The contact condition between the cutting tool and workpiece materials affect the estimation of HTC greatly. Moreover, HTC is dependent on the surface temperature [19]. But the temperature scope in the given machining process is limited, so the temperature-dependent HTC is difficult to obtain in a certain machining process.

In this study, heat transfer coefficients (HTCs) of different cooling processes, including nature cooling, compressed air cooling, compressed cold-air cooling, minimal quantity lubrication (MQL) cooling, and atomizing water cooling, have been estimated. Cemented carbide cutting inserts with block shape are used as a measured objective. The temperature changes of inserts in cooling processes are measured by infrared (IR) pyrometer. The temperature-dependent emissivity is measured to ensure the precision of the measured temperature. The effect of surface temperature, temperature of coolant carrier, and air velocity of coolant carrier on HTCs is considered. The finite element method (FEM) is employed to simulate the cooling process and modify the estimated heat transfer coefficients.

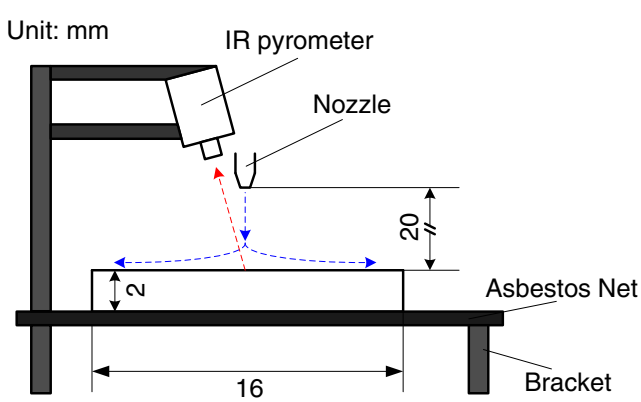

Fig. 2 Schematic of the experiment set

Table 2 Cooling conditions

Cooling medium	Carrier temperature (°C)	Carrier velocity (m/s)	Oil quantity (ml/h)
Nature cooling	25	–	–
Compressed air	25	4	–
		8	–
		16	–
		32	–
Compressed cold air	−20	4	–
		8	–
		16	–
		32	–
MQL	25	8	5
			10
			15
			20
MQL	−20	8	5
			10
			15
			20
AWL	25	8	5
			10
			15
			20

2 Temperature measurement by infrared pyrometer

The different methods of temperature measurement also affect the estimation of HTC. Nowadays, there are several experimental techniques available for temperature measurement, such as thermocouples, infrared (IR) pyrometers, thermosensitive coating, and metallurgical inspection [24]. Thermocouple method is widely used to measure the average temperature of a certain area. But thermocouple which is fixed on the surface may affect the temperature distribution of the surface, especially the maximal temperature on the surface. In

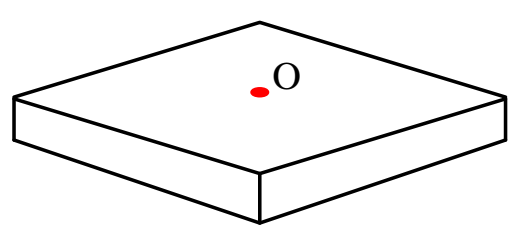

Fig. 3 Cutting insert and the position of temperature measurement

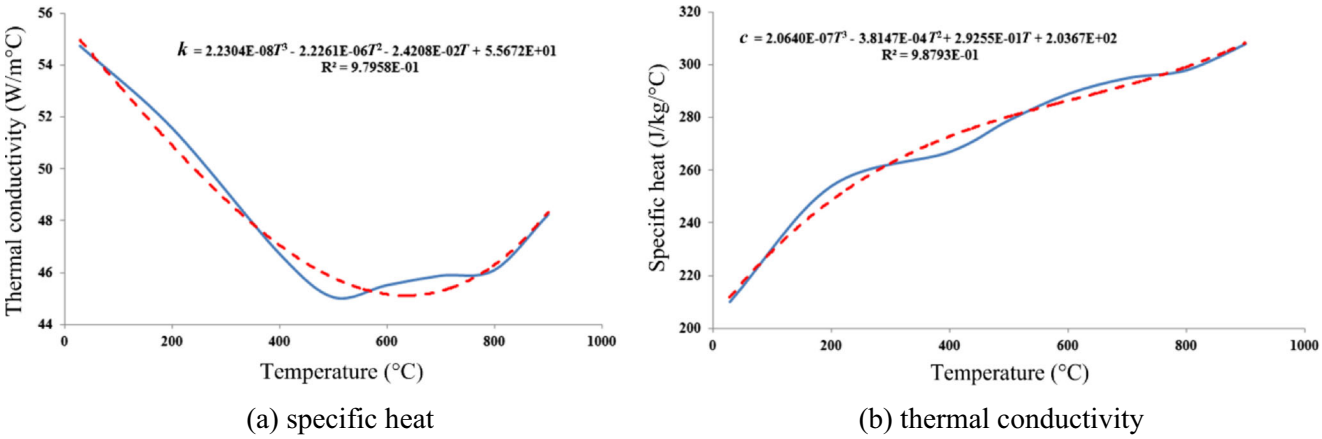

(a) specific heat (b) thermal conductivity

Fig. 4 Temperature-dependent thermal properties of cemented carbide. **a** Specific heat. **b** Thermal conductivity

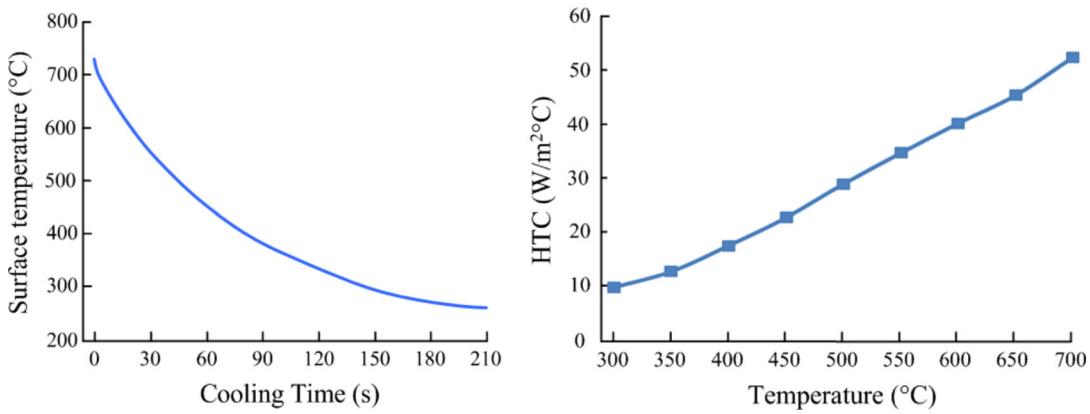

(a) Cooling curve of natural cooling (b) Calculated heat transfer coefficients of natural cooling

Fig. 5 Typical cooling curve and calculated heat transfer coefficients of nature cooling. **a** Cooling curve of natural cooling. **b** Calculated heat transfer coefficients of natural cooling

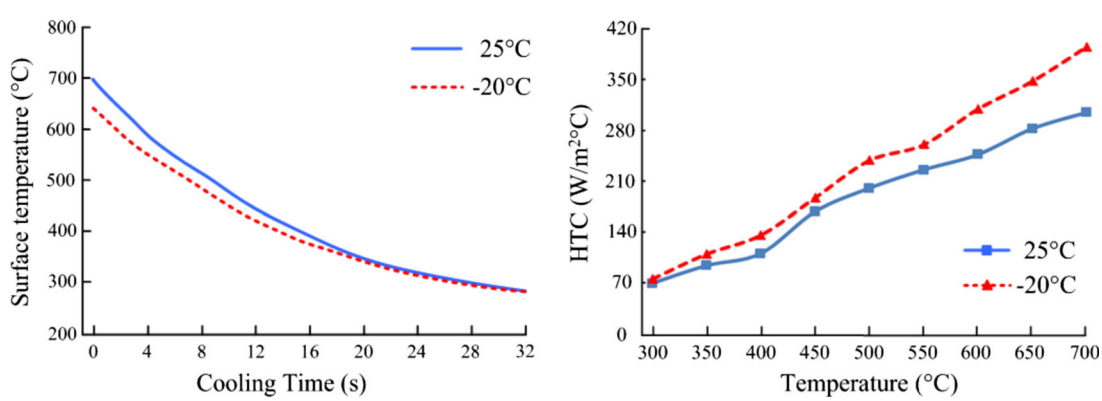

(a) Cooling curve of compressed air cooling (b) Calculated heat transfer coefficients of compressed air cooling

Fig. 6 Typical cooling curve and calculated heat transfer coefficients of compressed air cooling (air velocity 8 m/s, *solid line*: compressed air cooling, *dash line*: forced cold air cooling). **a** Cooling curve of compressed air cooling. **b** Calculated heat transfer coefficients of compressed air cooling

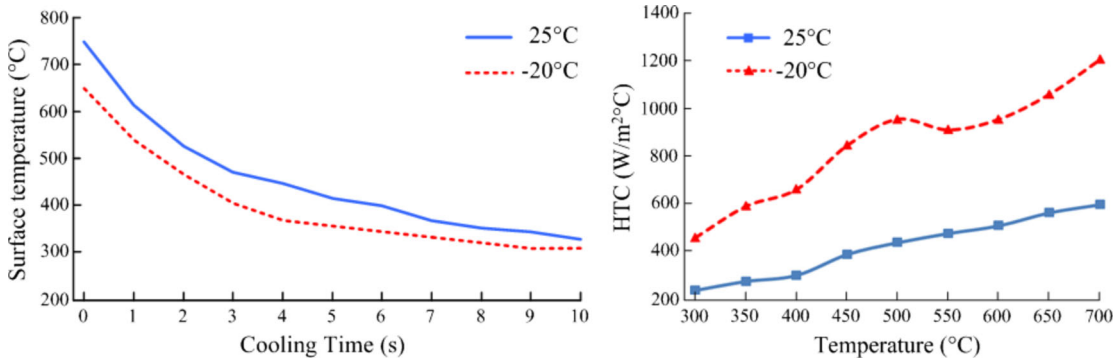

(a) Cooling curve of MQL with oil (b) Calculated heat transfer coefficients of MQL with oil

Fig. 7 Typical cooling curve and calculated heat transfer coefficients of MQL with oil (air velocity 8 m/s, oil quantity 10 ml/h, *solid line*: MQL with normal air, *dash line*: MQL with cold air). **a** Cooling curve of MQL with oil. **b** Calculated heat transfer coefficients of MQL with oil

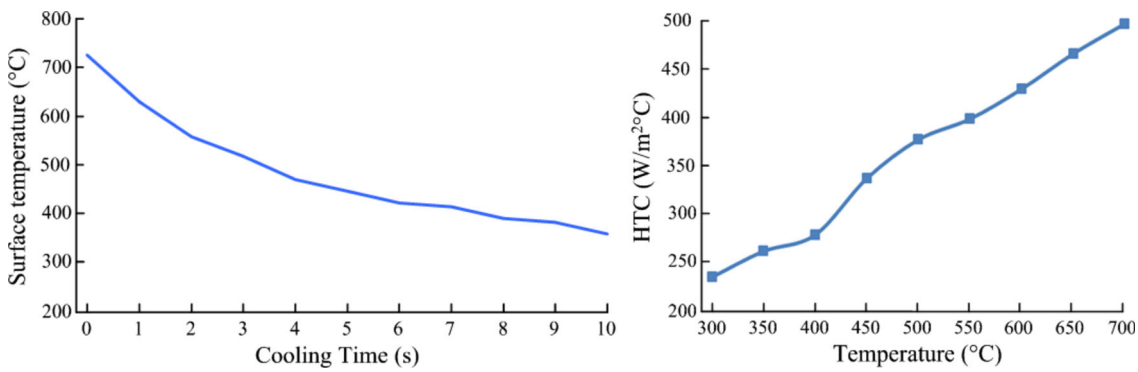

(a) Cooling curve of MQL with water (b) Calculated heat transfer coefficients of MQL with water

Fig. 8 Typical cooling curve and calculated heat transfer coefficients of MQL with water (air velocity 8 m/s, oil quantity: 10 ml/h). **a** Cooling curve of MQL with water. **b** Calculated heat transfer coefficients of MQL with water

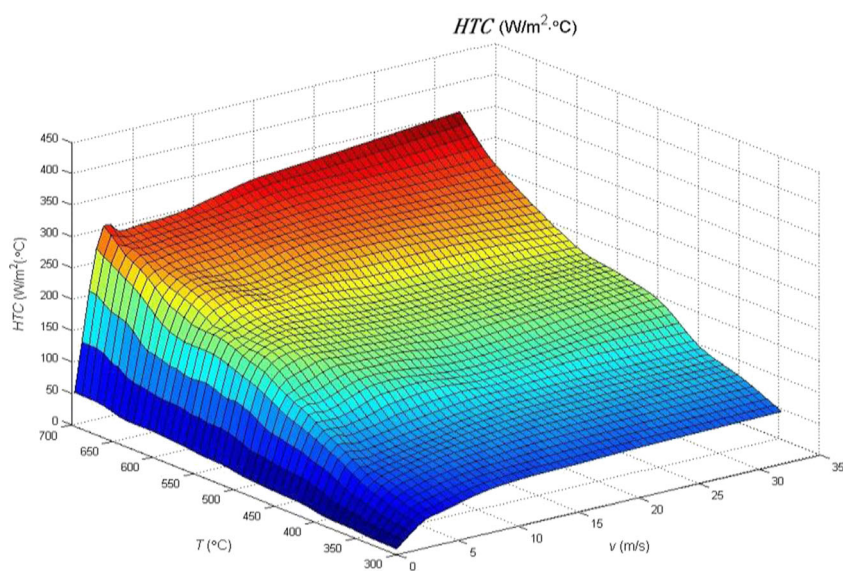

Fig. 9 Heat transfer coefficients of natural and compressed air cooling (25 °C)

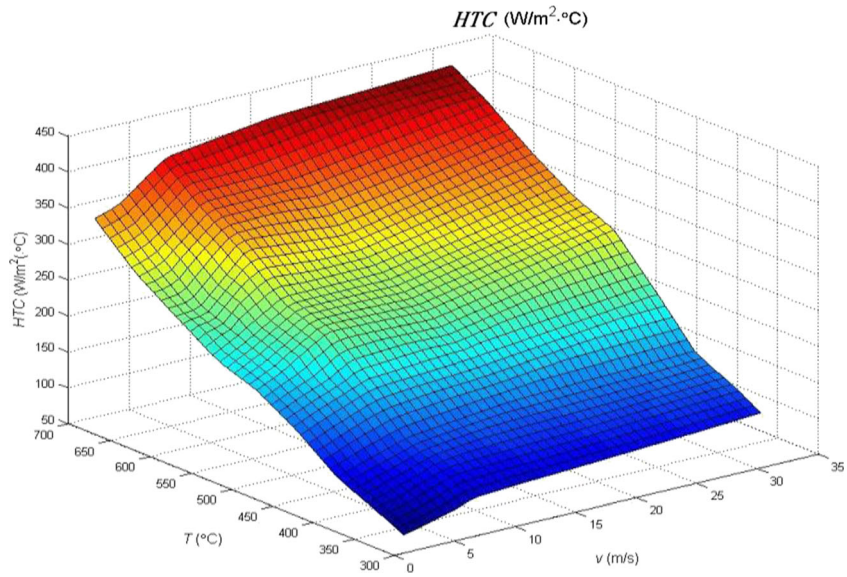

Fig. 10 Heat transfer coefficients of compressed cold air cooling (−20 °C)

this study, the maximal temperature of the measured surface is required. The cooling media used in near-dry cutting may not block the radiation from the surface measured. Therefore, the IR pyrometer method is the best choice.

IR pyrometer receives and measures the radiation energy from object surface. Stefan-Boltzmann law is employed to calculate the surface temperature with the given emissivity:

$$E = \varepsilon \cdot \sigma \cdot T^4 \tag{1}$$

where ε is the emissivity of an object, which depends on the surface properties and surface temperature. σ is Stefan-Boltzmann constant which is equal to 5.67E-10. T is the temperature of object surface. E is the radiation energy in the unit area of object surface.

Emissivity of object ε is very important for the precision of measured temperature. So the calibration for the emissivity of cemented carbide (material of measured cutting tool) is performed first. The calibration procedures are as follow:

- The thermal couple with a diameter of 0.5 mm is fixed on the surface of cemented carbide inserts.
- The blocks of cemented carbide K30 with thermal couple are heated in the resistance furnace to about 300, 400, 500, 600, 700, and 800 °C, respectively.
- The blocks are taken out and put on a bracket with an asbestos net under them.

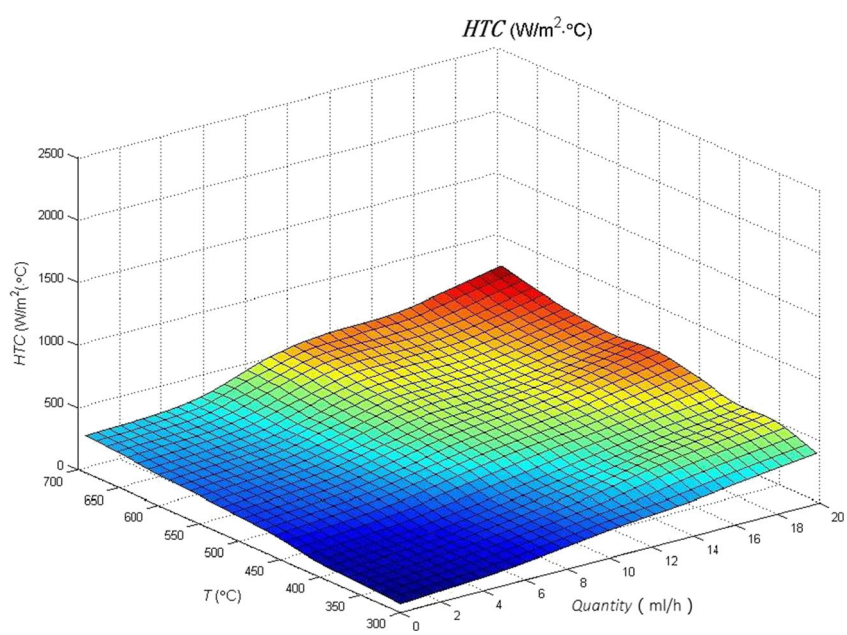

Fig. 11 Heat transfer coefficients of MQL (25 °C)

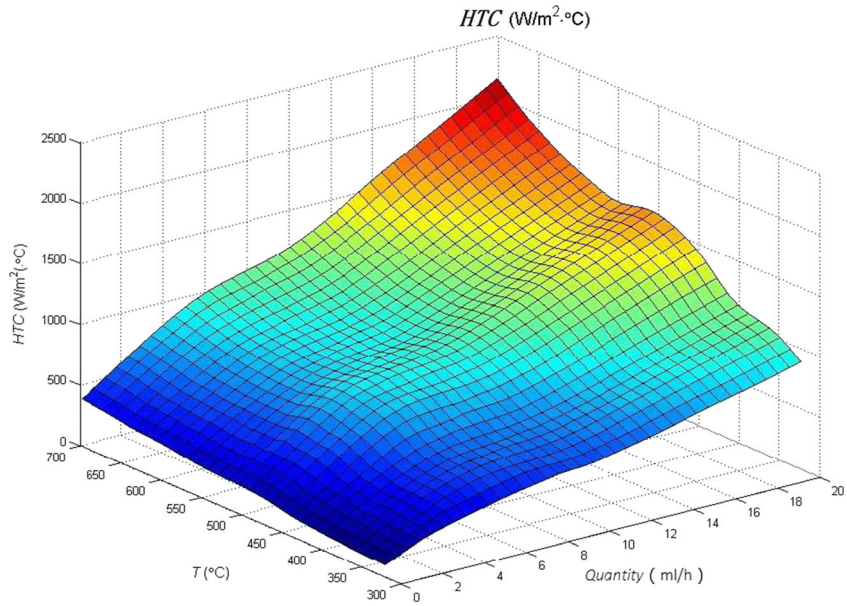

Fig. 12 Heat transfer coefficients of in MQL (−20 °C)

- The thermal couple records the temperature during the cooling process. And IR pyrometer records the thermal images during the cooling process at the same time. The measurement processes' finish temperature drop is about 50 °C.
- The energy from the IR pyrometer and the temperature from the thermal couple are in the same position of sample surface and at the same time are used to calculate the average emissivity in the different surface temperatures.

The temperature-dependent emissivity is shown in Fig. 1. The emissivity increases with the increase of surface temperature. The relationship between emissivity and temperature is expressed as cubic term.

3 Cooling conditions

It always pays more attention on the temperature of cutting tool than the temperature of workpiece due to control of tool wear. So it focuses on heat transfer analysis of cutting tool in this study. The cemented carbide blocks with a dimension 16*16*2 mm are selected. The material is K30 cemented carbide, which is widely used as a cutting tool material. The top surface (measure surface) is polished to Ra 0.1 μm. The samples are heated in the resistance furnace to about 800 °C and then put on a bracket with asbestos net under it. Cooling nozzle is vertical to the top surface of the sample. The inner diameter of the nozzle is 4 mm. The air velocity and

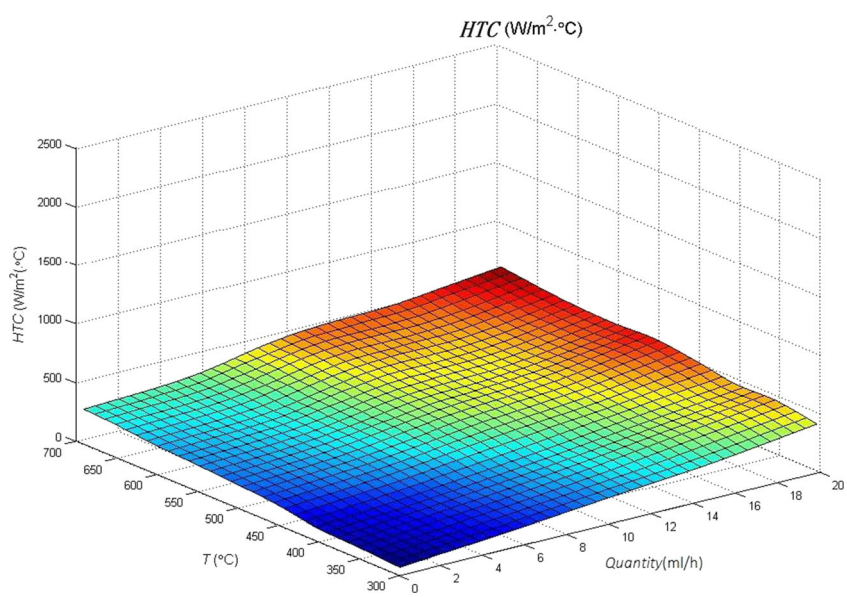

Fig. 13 Heat transfer coefficients of AWL (25 °C)

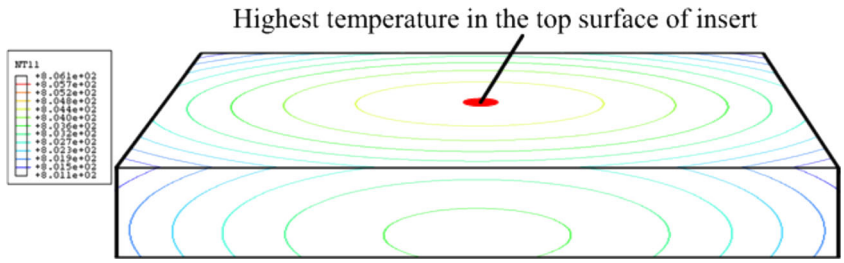

Fig. 14 FEM-simulated results

temperature are measured by type KA33 hot wire air velocity and temperature meter of Kanomax Company. A NEC IR pyrometer R300 is used to record the thermal images during the cooling process. Sampling interval is 0.1 s. A cold air generation machine with MQL system is employed to produce different cooling conditions. The oil used for MQL is a kind of low-temperature synthetic oil with boiling point 280~320 °C and condensation point −40 °C. The experiment set is shown in Fig. 2.

The cooling conditions are listed in Table 2.

4 Results and discussions

The maximal temperature of inserts during the cooling process is located in the center of the top face, point O in Fig. 3. The temperature of point O is always the maximal temperature in the thermal image from the IR pyrometer. The change of maximal temperature in the thermal image is recorded.

It is assumed that the maximal temperature is T_1 in the cooling time t_1 while T_2 in the cooling time t_2. The heat transfer coefficient of temperature $(T_1+ T_2)/2$ of insert is expressed as

$$h_{\frac{T_1+T_2}{2}} = \frac{c_{\frac{T_1+T_2}{2}}\rho v(T_1-T)_2}{A(t_2-t_1)\left(\frac{T_1+T_2}{2}-T_{\text{ambient}}\right)} \tag{2}$$

where A is the convection area, T_1 and T_2 are the surface temperatures in the cooling time t_1 and t_2, T_{ambient} is the ambient temperature, which is approximately considered as the cold-air temperature (−20 °C) in cold-air cutting and room temperature (25 °C) in other cooling conditions. V_2 is the volume of sample

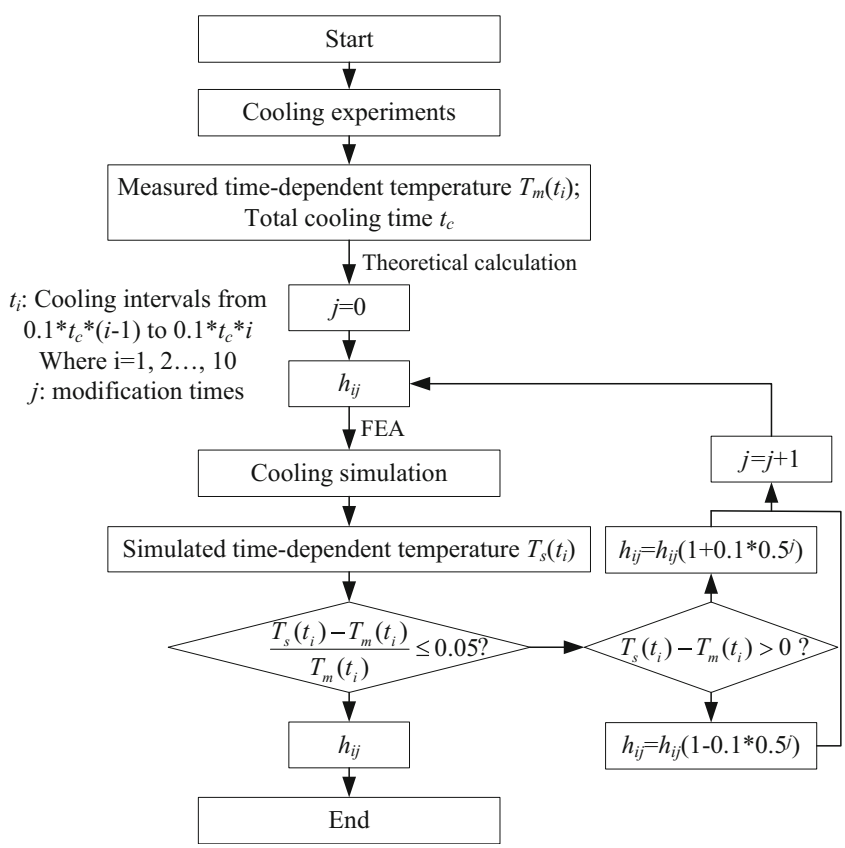

Fig. 15 Flow chart of modification

Table 3 Estimated and modified heat transfer coefficients in natural and compressed air cooling of room temperature

T (°C)	Heat transfer coefficients (W/m^2 °C)											
	Natural cooling		Compressed air cooling 25 °C, 2 m/s		Compressed air cooling 25 °C, 4 m/s		Compressed air cooling 25 °C, 8 m/s		Compressed air cooling 25 °C, 16 m/s		Compressed air cooling 25 °C, 32 m/s	
	Estimated	Modified	Estimated	Modified	Estimated	Modified	Estimated	Modified	Estimated	Modified	Estimated	Modified
300	9.4	9.3	41.1	48.1	53.0	56.8	70.0	66.5	77.5	80.3	84.4	88.3
350	12.5	12.3	62.5	69.4	79.3	82.4	94.0	90.6	105.7	107.3	113.0	114.7
400	17.6	17.3	97.9	93.8	97.9	102.3	110.4	113.5	128.6	128.0	134.3	135.8
450	23.1	22.8	130.8	135.8	143.1	136.7	166.9	142.4	156.4	176.6	182.9	178.2
500	29.7	29.3	166.0	167.3	198.9	160.6	198.7	171.9	192.0	210.5	200.5	201.6
550	35.8	35.3	189.8	190.1	211.4	176.8	223.5	190.9	213.9	226.7	214.5	217.2
600	41.7	41.1	197.3	203.5	246.3	214.5	244.3	224.6	262.6	258.1	249.7	251.0
650	47.2	46.5	247.5	243.5	271.1	247.1	279.3	256.9	291.6	294.9	293.1	289.1
700	54.7	53.9	292.9	275.2	295.1	297.1	301.3	298.9	332.9	340.8	362.9	346.0

block with a value of 512 mm^3. ρ is the density of K30 cemented carbide material with a value of 14.1 g/cm^3. c is the specific heat, which is temperature dependent.

Most researchers consider that thermal properties, including specific heat and thermal conductivity, for cutting tool material and workpiece material are kept constant because of their slight variation in the studied temperature range. The temperature range in this study is wide, so the temperature-dependent thermal properties of cemented carbide material are measured by Netzsch LFA 457 MicroFlash, as shown in Fig. 4. The relationship between thermal properties and temperature is expressed as cubic term, which could be used in Eq. (2).

The measured cooling curve and calculated HTC are shown in Figs. 5, 6, 7, and 8.

It is found that HTC increases with the increase of surface temperature in all the cooling conditions. Cold air could increase HTC, especially in MQL cooling condition. The reason is that the coolant is present from high-temperature deterioration before the coolant arrives at a cooled surface. HTC of water mist cooling is much lower that of HTC of oil mist cooling. The reason is that the boiling point of water is much lower than oil; subsequently less water mist arrives at the cooled surface, so less heat is removed by water mist, compared with oil mist.

The estimated HTC are shown in Figs. 9, 10, 11, 12, and 13.

It is found that HTC has an increased trend with the increase of air velocity in compressed (cold) air cooling. But the effect of air velocity on HTC is limited. Actually, during the

Table 4 Estimated and modified heat transfer coefficients in compressed cold air cooling (−20 °C)

T (°C)	Heat transfer coefficients (W/m^2 °C)									
	Compressed air cooling −20 °C, 2 m/s		Compressed air cooling −20 °C, 4 m/s		Compressed air cooling −20 °C, 8 m/s		Compressed air cooling −20 °C, 16 m/s		Compressed air cooling −20 °C, 32 m/s	
	Estimated	Modified	Estimated	Modified	Estimated	Modified	Estimated	Modified	Estimated	Modified
300	48.8	52.6	57.5	60.9	75.5	78.3	83.8	86.9	99.1	98.9
350	77.3	78.7	84.5	88.5	109.5	109.3	115.8	117.8	132.9	130.7
400	101.9	103.9	114.0	113.3	135.0	134.1	150.2	149.3	159.6	155.9
450	144.7	147.6	159.4	155.9	185.4	180.1	194.7	189.7	223.8	212.4
500	178.5	181.4	194.4	200.9	236.1	228.6	232.7	226.8	285.3	258.0
550	198.7	203.4	216.6	218.7	257.5	251.7	258.3	251.3	309.4	279.0
600	236.7	231.5	240.0	252.1	305.9	294.3	293.8	289.4	346.0	316.1
650	275.5	271.9	287.3	287.8	343.5	329.7	345.7	335.7	387.9	358.1
700	328.0	316.7	338.6	328.5	390.3	367.7	409.3	393.8	422.6	405.6

Table 5 Estimated and modified heat transfer coefficients in MQL (25 °C)

T (°C)	Heat transfer coefficients (W/m^2 °C)									
	MQL, compressed air cooling 25 °C, 0 ml/h, 8 m/s		MQL, compressed air cooling 25 °C, 5 ml/h, 8 m/s		MQL, compressed air cooling 25 °C, 10 ml/h, 8 m/s		MQL, compressed air cooling 25 °C, 15 ml/h, 8 m/s		MQL, compressed air cooling 25 °C, 20 ml/h, 8 m/s	
	Estimated	Modified	Estimated	Modified	Estimated	Modified	Estimated	Modified	Estimated	Modified
300	70.0	66.5	123.1	96.5	224.0	204.2	305.0	284.5	406.9	380.9
350	94.0	90.6	152.9	120.6	262.4	240.7	416.3	376.6	518.0	487.2
400	110.4	113.5	169.5	143.5	288.6	275.9	424.3	388.3	516.8	480.8
450	166.9	142.4	239.0	172.4	379.0	317.7	479.7	437.2	598.9	549.7
500	198.7	171.9	271.0	201.9	429.9	360.1	518.2	473.9	658.8	598.7
550	223.5	190.9	291.9	220.9	469.6	391.0	509.1	466.8	636.0	573.0
600	244.3	224.6	306.4	254.6	502.9	438.0	532.1	489.1	667.0	599.2
650	279.3	256.9	336.4	286.9	558.9	483.6	582.3	530.9	725.7	646.6
700	301.3	298.9	349.8	328.9	594.1	539.8	653.4	589.7	808.9	718.7

air cooling of sample block, the air velocity is vertical to the surface of cutting tool, so the convention velocity on the surface of cutting tool is much less than the air velocity from nozzle, as shown in Fig. 2. With the given power of air cooling machine, the pressure is inversely proportional to flow rate, which determines the air velocity. Because the air velocity has little influence on the heat transfer coefficient, a higher pressure can be selected to increase the outlet pressure and decrease the adhesion loss of oil mist and carry the oil mist to the closer position of the cutting point.

It is found that HTC has an increased trend with the increase of oil mist in the cooling condition of MQL. Compared with regular MQL, the HTC increases by even 150 % in cooling condition of cold air MQL due to performance protect of oil mist by cold air. It is found that HTC of AWL is much lower than that of MQL in the same condition. However, cooling ability of water is stronger than that of oil. The reason is that most water mist is evaporated far away from the cooled surface due to high temperature. So the actual cooling media is basically water vapor.

5 Modification method of HTC based on FEA

In the theoretical model, it is assumed the heat transfer accords with the steady-state one-dimensional heat transfer and no energy is lost from heat radiation. These assumptions can result in the error in the estimation of heat transfer coefficients. So a finite element model is built to simulate the cooling

Table 6 Estimated and modified heat transfer coefficients in MQL (−20 °C)

T (°C)	Heat transfer coefficients (W/m^2 °C)									
	MQL, compressed air cooling −20 °C, 0 ml/h, 8 m/s		MQL, compressed air cooling −20 °C, 5 ml/h, 8 m/s		MQL, compressed air cooling −20 °C, 10 ml/h, 8 m/s		MQL, compressed air cooling −20 °C, 15 ml/h, 8 m/s		MQL, compressed air cooling −20 °C, 20 ml/h, 8 m/s	
	Estimated	Modified	Estimated	Modified	Estimated	Modified	Estimated	Modified	Estimated	Modified
300	75.5	78.3	293.4	282.1	452.3	426.4	626.3	555.2	812.2	642.1
350	109.5	109.3	485.4	469.7	587.5	539.1	815.1	773.8	1056.1	956.1
400	135.0	134.1	538.3	521.4	660.7	602.9	904.2	841.7	1163.8	1048.4
450	185.4	180.1	718.1	691.0	850.6	811.8	1153.1	1072.5	1474.6	1357.2
500	236.1	228.6	791.0	752.7	964.1	822.2	1299.3	1101.0	1630.4	1367.5
550	257.5	251.7	735.2	696.4	917.9	794.4	1254.7	1031.3	1585.4	1327.8
600	305.9	294.3	763.5	714.2	963.9	865.7	1341.2	1100.6	1706.1	1442.2
650	343.5	329.7	833.2	775.9	1071.7	978.7	1495.8	1228.8	1913.3	1631.9
700	390.3	367.7	941.0	871.6	1221.6	1136.1	1705.3	1417.8	2193.0	1890.3

Table 7 Estimated and modified heat transfer coefficients in AWL (25 °C)

T (°C)	Heat transfer coefficients (W/m^2·°C)									
	AWL, compressed air cooling 25 °C, 0 ml/h, 8 m/s		AWL, compressed air cooling 25 °C, 5 ml/h, 8 m/s		AWL, compressed air cooling 25 °C, 10 ml/h, 8 m/s		AWL, compressed air cooling 25 °C, 15 ml/h, 8 m/s		AWL, compressed air cooling 25 °C, 20 ml/h, 8 m/s	
	Estimated	Modified	Estimated	Modified	Estimated	Modified	Estimated	Modified	Estimated	Modified
300	70.0	66.5	140.3	133.7	224.7	216.2	306.9	293.2	421.8	398.6
350	94.0	90.6	163.7	154.6	253.4	242.5	367.3	343.4	477.3	450.8
400	110.4	113.5	181.8	173.4	271.8	265.0	377.2	353.8	473.2	443.4
450	166.9	142.4	234.2	204.2	334.7	301.4	415.9	387.2	529.4	489.2
500	198.7	171.9	262.7	236.4	378.0	339.4	443.0	412.8	573.3	519.6
550	223.5	190.9	279.3	249.8	401.1	358.8	439.9	410.3	557.1	500.4
600	244.3	224.6	293.2	278.3	434.4	396.2	457.9	429.2	574.0	515.1
650	279.3	256.9	326.8	307.4	473.7	429.2	497.7	462.1	607.4	543.0
700	301.3	298.9	354.2	343.7	507.2	468.7	553.9	509.2	649.5	585.9

processes and modify the estimated value of heat transfer coefficients.

The sample block is modelled as Fig. 14 shows. The heat convection and radiation conditions are applied in the top and four sides of the surface of the cutting insert. The adiabatic boundary condition is applied in the bottom surface to simulate the thermal barrier effect of asbestos net. The thermal properties of cemented carbide are modelled as temperature dependent, as shown in Fig. 4. FEM software ABAQUS 6.10 is employed to simulate the cooling processes.

The flow chart of modification is shown in Fig. 15. Total cooling time is divided into i intervals. $T_m(t_i)$, $T_s(t_i)$ and h_{ij} are, respectively, the measured maximal temperature, simulated maximal temperature, and heat transfer coefficients in the ith intervals. $T_m(t_i)$ and $T_s(t_i)$ is compared in every interval. If $(T_m(t_i) - T_s(t_i))/T_m(t_i) \leq 0.05$, the current h_{ij} is accepted; or else, the h_{ij} is modified and the simulations are performed again, as Fig. 5 shows. Finally, a group of modified h_{ij} is obtained and modification is completed.

Comparisons of estimated and modified heat transfer coefficients are listed in the Tables 3, 4, 5, 6, and 7.

6 Conclusion

Heat transfer coefficients (HTCs) of different cooling processes, including nature cooling, compressed air cooling, compressed cold air cooling, minimal quantity lubrication (MQL) cooling, and atomizing water cooling, have been estimated and modified by FEM.

It is found that HTC is from 9.3 to 53.9 W/m^2/°C with different surface temperatures in nature cooling. HTC increases with the increase of surface temperature. HTC is from 48.1 to 346.0 W/m^2/°C with different air velocity and surface temperature in compressed air cooling. HTC has an increased trend with the increase of air velocity. HTC is from 52.6 to 405.6 W/m^2/°C with different air velocities and surface temperatures in compressed cold air cooling. Lower air temperature increases HTC by 10~20 %. HTC is from 96.5 to 718.7 W/m^2/°C with different oil quantities and surface temperatures in MQL cooling. HTC increases with the increase of oil quantity of MQL. As a comparison, HTC is from 133.7 to 519.6 W/m^2/°C with different water quantities and surface temperatures in AWL cooling. HTC of AWL is much lower than that of MQL in the same condition, especially when the surface temperature is high. The boiling point of water is much lower than oil; subsequently, less water mist arrives at the cooled surface, so less heat is removed with AWL cooling than that with MQL cooling in the same condition. HTC is from 282.1 to 1890.3 W/m^2/°C with different oil quantities and surface temperature in cold air MQL cooling. Lower carrier temperature increases the HTC greatly, even increases the HTC by 150 % when the surface temperature is up to 700 °C. The reason is that the coolant prevents high-temperature deterioration before the coolant arrives at cooled surface.

Acknowledgments The authors gratefully acknowledge the financial support by the National Natural Science Foundation (No. 51475173, 51235004 and U1305241) and the Major Project on the Integration of Industry and Research of Fujian Province (No. 2014H6018).

References

1. Su Y, He N, Li L, Li XL (2006) An experimental investigation of effects of cooling/lubrication conditions on tool wear in high-speed end milling of Ti-6Al-4V. Wear 261:760–766. doi:10.1016/j.wear.2006.01.013

2. Wakabayashi T, Suda S, Inasaki I, Terasaka K, Musha Y, Toda Y (2007) Tribological action and cutting performance of MQL media in machining of aluminum. CIRP Ann Manuf Technol 56:97–100. doi:10.1016/j.cirp.2007.05.025
3. Zhang Y, Jun MBG (2013) Mixed jet of independently atomized water and oil sprays as cutting fluids in micro-milling. Manuf Lett 1:13–16. doi:10.1016/j.mfglet.2013.08.003
4. Yokogawa K, Yokogawa M, Okumura S (1998) Cooling air grinding and cutting technology. Tool Eng 42:57–62
5. Hong SYDY (2001) Cooling approaches and cutting temperatures in cryogenic machining of Ti-6Al-4V. Int J Mach Tools Manuf 41: 1417–1437
6. Jiang F, Li J, Yan L, Sun J, Zhang S (2010) Optimizing end-milling parameters for surface roughness under different cooling/lubrication conditions. Int J Adv Manuf Technol 51:841–851. doi:10.1007/s00170-010-2680-9
7. Hadad M, Sadeghi B (2013) Minimum quantity lubrication-MQL turning of AISI 4140 steel alloy. J Clean Prod 54:332–343. doi:10.1016/j.jclepro.2013.05.011
8. Astakhov VP, Joksch S.(2012) Metalworking fluids (Mwfs) for cutting and grinding: fundamentals and recent advances
9. Yamazaki T, Miki K, Sato U (2003) Cooling air cutting of Ti-6Al-4V alloy. J Jpn Inst Light Metals 53:416–420
10. Wang S, Clarens AF (2013) Analytical model of metalworking fluid penetration into the flank contact zone in orthogonal cutting. J Manuf Process 15:41–50. doi:10.1016/j.jmapro.2012.09.015
11. Ueda T, Hosokawa A, Yamada K (2006) Effect of oil mist on tool temperature in cutting. ASME J Manuf Sci Eng 128:130–135
12. Hadad M, Sadeghi B (2012) Thermal analysis of minimum quantity lubrication-MQL grinding process. Int J Mach Tools Manuf 63:1–15. doi:10.1016/j.ijmachtools.2012.07.003
13. Atlati S, Haddag B, Nouari M, Zenasni M (2014) Thermomechanical modelling of the tool–work material interface in machining and its implementation using the ABAQUS VUINTER subroutine. Int J Mech Sci 87:102–117. doi:10.1016/j.ijmecsci.2014.05.034
14. Ceretti E, Filice L, Umbrello D, Micari F (2007) ALE simulation of orthogonal cutting: a new approach to model heat transfer phenomena at the tool-chip interface. CIRP Ann Manuf Technol 56:69–72. doi:10.1016/j.cirp.2007.05.019
15. Brandão LC, Coelho RT, Malavolta AT (2010) Experimental and theoretical study on workpiece temperature when tapping hardened AISI H13 using different cooling systems. J Braz Soc Mech Sci Eng 32:154–159
16. Brandao LC, Coelho RT, Lauro CH (2011) Contribution to dynamic characteristics of the cutting temperature in the drilling process considering one dimension heat flow. Appl Therm Eng 31:3806–3813. doi:10.1016/j.applthermaleng.2011.07.024
17. Luchesi VM, Coelho RT (2012) Experimental investigations of heat transfer coefficients of cutting fluids in metal cutting processes: analysis of workpiece phenomena in a given case study. Proc Inst Mech Eng 226
18. Kops L, Arenson M (1999) Determination of convective cooling conditions in turning. CIRP Ann Manuf Technol 48:47–52. doi:10.1016/S0007-8506(07)63129-1
19. Jiang F, Li J, Sun J, Al E (2010) Estimation of heat transfer coefficients in dry and cold-air cutting. Adv Mater Res 126-128:341–346
20. Umbrello D, Filice L, Rizzuti S, Micari F (2007) On the evaluation of the global heat transfer coefficient in cutting. Int J Mach Tools Manuf 47:1738–1743. doi:10.1016/j.ijmachtools.2006.12.002
21. Barrios ANS, Silva JBC, Rodrigues AR, Coelho RT, Braghini Junior A, Matsumoto H (2014) Modeling heat transfer in die milling. Appl Therm Eng 64:108–116. doi:10.1016/j.applthermaleng.2013.12.015
22. Lincoln Cardoso Brandão RTCA (2008) Experimental and theoretical study of workpiece temperature when end milling hardened steels using (TiAl)N-coated and PcBN-tipped tools. J Mater Process Technol 199:234–244
23. Cheng G, Han F, Feng Z (2007) Experimental determination of convective heat transfer coefficient in WEDM. Int J Mach Tools Manuf 47:1744–1751. doi:10.1016/j.ijmachtools.2006.12.003
24. Lin J, Liu CY (2001) Measurement of cutting tool temperature by an infrared pyrometer. Meas Sci Technol 1243–1249